PHYSICAL REVIEW B VOLUME 32, NUMBER 8 15 OCTOBER 1985

Electron subbands and transport properties in inversion layers of InAs and InP

Eiichi Yamaguchi
*Nippon Telegraph and Telephone Electrical Communication Laboratories, Musashino-shi, Tokyo 180, Japan**
and Department of Physics, University of Notre Dame, Notre Dame, Indiana 46556
(Received 12 October 1984; revised manuscript received 17 June 1985)

Subband structures and electron transport are systematically investigated in the two-dimensional inversion layers on InAs and InP metal-insulator-semiconductor field-effect transistors. Hybrid quantum oscillations of conductivity under a strong magnetic field reveal that the two-subband conduction state is realized above an electron concentration N_s of 1.4×10^{12} and 3.8×10^{12} cm^{-2} for InAs (acceptor concentration $N_A=1\times10^{17}$ cm^{-3}) and InP ($N_A=1.7\times10^{16}$ cm^{-3}), respectively. Field-effect mobility is observed to decrease abruptly at the onset of the two-subband conduction state at low temperatures. This remarkable effect is due to intersubband scattering. Electron mobility in inversion layers on these III-V compounds is also found to be limited mainly by three scattering mechanisms: screened Coulomb scattering due to the charged interface states at low N_s values, defect scattering due to the out-diffusion of group-V atoms at intermediate N_s values, and surface roughness scattering at high N_s values. Additionally, negative magnetoresistance is observed due to the weak localization effect in the two-dimensional systems. Positive magnetoresistance is also observed in InAs, due to the spin-orbit interaction with a large absolute value of an effective g factor. Finally, intersubband scattering is found to give rise to a remarkable effect on the weak localization.

I. INTRODUCTION

Many efforts have recently been devoted to the preparation of metal-insulator-semiconductor field-effect transistors (MISFET's) onto III-V compound semiconductors, especially InP,[1–10] $In_xGa_{1-x}As_yP_{1-y}$,[11–13] and InAs.[14–16] However, their fabrication technology was lagged so far behind, that investigations on transport properties are still in the initial stage on these MISFET's. Fortunately, natural two-dimensional electron-gas (2DEG) layers are formed on surface or interface of InAs. Tsui,[17–21] Sakaki *et al.*,[22] Washburn and Sites,[23] and Washburn *et al.*[24] extensively studied n-channel accumulation layers of InAs. However, a few investigations have been performed on n-channel inversion layers of InAs.[25,26]

Very recently, magnetoconductance studies have for the first time, revealed the two-dimensionality in the n-channel inversion layers on InAs (Ref. 16) and InP (Refs. 27–29) MIS structures. Subband structures and their effect on electron transport have also been investigated in the 2DEG systems on InAs (Ref. 16) and InP (Ref. 29) MISFET's.

The present work is a continuation of the experiments first reported in Refs. 16 and 29, in which the subband structures and transport properties in the 2DEG inversion layers are compiled on InAs and InP MISFET's. Section II describes the sample-preparation technique. Section III presents the experimental results on the Shubnikov–de Haas effect, mobilities as functions of electron concentration and temperature, and the magnetoresistance effect. This section also involves a brief discussion of Anderson localization and its effect on transport properties in 2DEG systems on both InAs and InP. Section IV summarizes the conclusions on this work.

II. EXPERIMENTAL TECHNIQUE

Substrates used in this experiment were Zn-doped p-type InAs and InP crystals with 1×10^{17} cm^{-3} and 1.7×10^{16} cm^{-3} acceptor concentration, respectively. After the wafers with [100] orientations were polished mechanochemically with a Br-methanol solution, the surfaces were prepared by the following steps; a thorough rinsing in acetone and water, a 10-s etch in a mixture of H_2SO_4, H_2O_2, and H_2O (2:1:1), and a 30-s etch in Br-methanol solution

In the InAs samples, native inversion layers formed with contact to Au-Ge-Ni (8:1:1) were used as source and drain n-type regions. On the other hand, in the InP samples, source and drain regions were formed by Si^+ implantation with a 2×10^{14} cm^{-2} dose at 200 keV, and subsequent annealing at 650 °C for 15 min with an SiO_2 encapsulation. Following this, source and drain electrodes were formed by evaporating Au-Ge-Ni (8:1:1) in the InP. Here, for both semiconductor samples, these electrodes had Corbino-disk structures with an inner radius r_i of

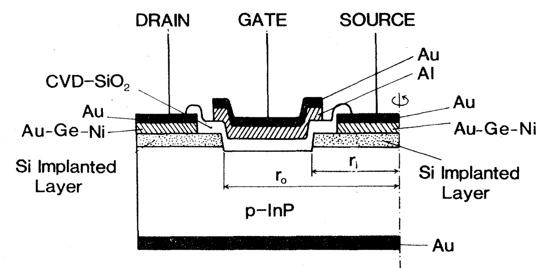

FIG. 1. Schematic view of the InP MISFET sample.

 ©1985 The American Physical Society

TABLE I. InAs and InP samples.

Substrate	Sample label	T_D (°C)	r_0 (μm)	r_i (μm)
p-InAs	A-1	187—200	370	160
	A-2	225—240	370	160
	A-2a	265—280	370	112
	A-3	359—377	370	160
p-InP	P-1	245—260	370	210

112—210 μm and an outer radius r_0 of 370 μm, respectively.

The SiO_2 film was deposited pyrolytically at several deposition temperatures, T_D, as a gate insulator. The devices were completed by the deposition of Al and Au for a gate electrode. Figure 1 shows a schematic view of the InP sample. Table I allows an identification of the samples and their labels as employed in Sec. III, where the sample with "a" at the end of the label (as in A-2a) has an anodic oxide film (thickness $\simeq$200 Å) as an inner gate insulator.[16,29] The fabricated InAs and InP MISFET's were mounted and wire bonded on dual-in-package (DIP) headers and set in a cryostat with a superconducting magnet. Conductivity measurement was made under a condition of constant source-drain field (3 V/cm) with a semiconductor parameter analyzer (HP4145A).

III. RESULTS AND DISCUSSION

A. Shubnikov—de Haas effect

Conductivity σ of 2DEG inversion layers were measured as a function of gate voltage V_g under a strong magnetic field at 1.6 K in the fabricated InAs and InP MISFET's. Figures 2(a) and 2(b) show the results in InAs and InP, respectively, where $d\sigma/dV_g$ is plotted versus V_g under various magnetic fields B. It can be seen in this figure that Shubnikov—de Haas (SdH) oscillation clearly occurs when surface Fermi level, E_{Fs}, meets each Landau level as in

$$E_n^{(\nu)}=E_\nu+\hbar\omega_c^{(\nu)}(n+1/2)$$

$$(n=0,1,2,\ldots;\ \nu=0,1,2,\ldots)\ , \quad (1)$$

where E_ν is the bottom energy of the νth subband, and $\omega_c^{(\nu)}=eB/m_e^{(\nu)}$ and is the cyclotron angular frequency with the νth subband electron effective mass, $m_e^{(\nu)}$. The conduction-electron concentration of each Landau level in the νth subband is given by

$$\Delta N_\nu=D_\nu(E)\hbar\omega_c^{(\nu)}=n_v eB/\pi\hbar\ , \quad (2)$$

where $D_\nu(E)=n_v m_e^{(\nu)}/\pi\hbar^2$ and is the 2DEG density of states, and n_v is the number of valley degeneracy. Therefore, when conduction-electron concentration, $N_{\rm inv}$ ($=\sum N_\nu$; N_ν is the conduction-electron concentration in the νth subband), is exactly equal to induced electron concentration N_s given by

$$N_s=C_i(V_g-V_{\rm th})/e \quad (3)$$

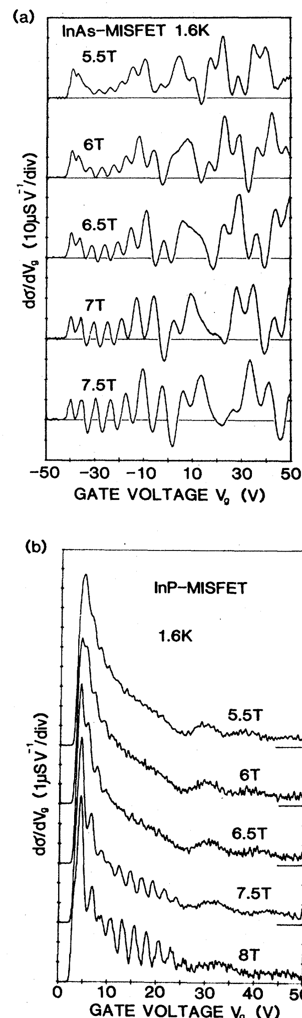

FIG. 2. Shubnikov—de Haas oscillations for $d\sigma/dV_g$ as a function of V_g under various magnetic fields, B, at 1.6 K in (a) InAs MISFET (A-2) and (b) InP MISFET (P-1).

with insulator capacitance C_i and threshold voltage $V_{\rm th}$, the period of gate voltage in the SdH oscillation is expressed

$$\Delta V_{g,0}=n_v e^2 B/\pi\hbar C_i \quad (4)$$

in the one-subband conduction state ($E_0\le E_{Fs}<E_1$).

In the multisubband conduction state ($E_\lambda\le E_{Fs}<E_{\lambda+1}$; $\lambda\ge 1$), Landau levels in each subband give a different period of observed gate voltage, $\Delta V_{g,\lambda}^{(\nu)}$ ($\nu=0,1,2,\ldots,\lambda$), which is, in general, a function of V_g, i.e., $N_{\rm inv}$. Each period $\Delta V_{g,\lambda}^{(\nu)}(N_{\rm inv})$ is given by $e\Delta N_{\rm inv}(N_{\rm inv})/C_i$ in terms of the concentration period of total inversion electrons, $\Delta N_{\rm inv}(N_{\rm inv})$, which gives a νth subband Landau level to be filled up. Using this relation, and Eqs. (2) and (4), the ratio of $\Delta V_{g,\lambda}^{(\nu)}(N_{\rm inv})$ to $\Delta V_{g,0}$ given by Eq. (4) can be written as

$$\Delta V_{g,\lambda}^{(\nu)}(N_{\rm inv})/\Delta V_{g,0}=\Delta N_{\rm inv}(N_{\rm inv})/\Delta N_\nu\ . \quad (5)$$

When the Landau levels originating from different subbands are not so well separated that $\Delta V_{g,\lambda}^{(\nu)}(N_{\rm inv})$ as well as

$\Delta N_{\rm inv}(N_{\rm inv})$ is sufficiently small, $\Delta N_{\rm inv}/\Delta N_\nu$ becomes almost equal to $dN_{\rm inv}/dN_\nu$. Then Eq. (5) approximately yields

$$\sum_{\nu=0}^{\lambda} 1/\Delta V_{g,\lambda}^{(\nu)}(N_{\rm inv}) = 1/\Delta V_{g,0} \tag{6}$$

for the subbands with the same n_ν.

Figure 3 illustrates the fan diagrams for the quantum oscillation shown in Fig. 2, where positions of gate voltage V_g at which $d\sigma/dV_g$ becomes minimum are plotted as a function of B. This fan diagram clearly shows that the quantum oscillations consist of two series of Landau levels, i.e., two quantized subbands in both MISFET's. The two threshold voltages, $V_{\rm th}^{(0)}$ $(=V_{\rm th})$ and $V_{\rm th}^{(1)}$, at which the surface Fermi level meets the bottom of each subband, can be accurately determined by extrapolating the plots to $B=0$. This is due to the fact that when the band-tailing effect is unimportant, each Landau level $E_n^{(\nu)}$ must become degenerated to the bottom of the subband, E_ν, as B approaches 0, as shown in Eq. (1). Further, the linearity in the extrapolation proves the relation $N_s = N_{\rm inv}$ for any V_g in both MISFET's.

A Fourier transformation (FT) of the data shown in Fig. 2 was made in order to accurately evaluate the period of oscillation. Figures 4(a) and 4(b) show the results, where Fourier power spectra are plotted versus $B/\Delta V_g$ under various B values. In Fig. 4(a), the solid and dashed lines, respectively, correspond to FT spectra within the regions -50 V $\le V_g < 50$ V and -50 V $\le V_g < -18$ V $(=V_{\rm th}^{(1)})$ in the InAs samples. Therefore, in Fig. 4(a) the peaks at 1.25 T/V of the dashed lines are equal to

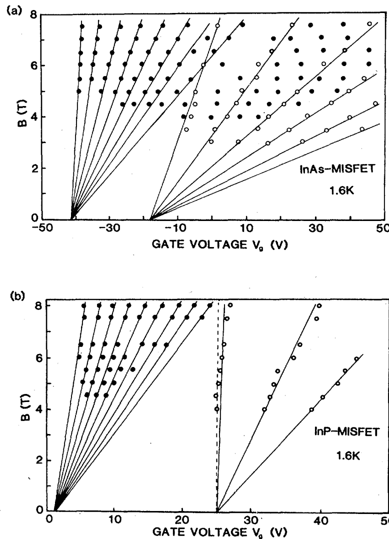

FIG. 3. Fan diagrams for the quantum oscillations shown in Fig. 2. Threshold voltages are estimated (a) at $V_{\rm th}^{(0)} = -41$ V and $V_{\rm th}^{(1)} = -18$ V for the InAs MISFET (A-2) and (b) at $V_{\rm th}^{(0)} = 1.2$ V and $V_{\rm th}^{(1)} = 25$ V for the InP MISFET (P-1). The dashed line in (b) corresponds to the line $V_g = V_{\rm th}^{(1)}$. The deviation of plots around $V_{\rm th}^{(1)}$ from the solid line toward the dashed line with a decrease in B is due to the effect of intersubband scattering.

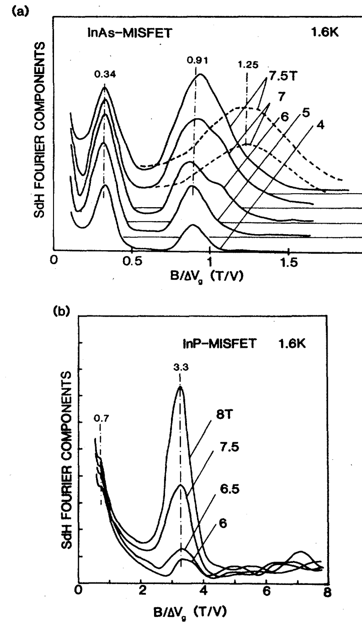

FIG. 4. Fourier power spectra as a function of $B/\Delta V_g$ for the SdH oscillation shown in Fig. 2.

$B/\Delta V_{g,0}$ in the one-subband conduction region, and those at 0.91 T/V and 0.34 T/V are equal to $B/\Delta V_{g,1}^{(0)}$ and $B/\Delta V_{g,1}^{(1)}$ respectively, in the two-subband conduction region in InAs. Note that for the solid lines each peak at 1.25 T/V disappears in the tail of spectrum around 0.91 T/V. This is because the sampling number in two-subband conduction region (-18 to 50 V) is sufficiently larger than that in one-subband conduction region (-50 to -18 V). It is found that these values actually satisfy the relation shown in Eq. (6).

On the other hand, Fig. 4(b) indicates that the peak which corresponds to $B/\Delta V_{g,1}^{(0)}$ is not observed in InP, because the InP MISFET has much lower mobility as is shown in the next section. The insulator capacitance C_i can also be determined to a point of high accuracy from these $B/\Delta V_{g,0}$ data, using Eq. (4), and was estimated at 9.69 and 25.6 nF/cm^2 for these InAs and InP samples, respectively.

Furthermore, conduction-electron concentration in each subband, N_ν, can be determined as a function of induced electron concentration, N_s, using Eq. (5). Figure 5(a) shows the result for two InAs samples, A-2 (solid circles) and A-2a (open circles). This figure illustrates that the two-subband conduction state realized above an N_s of 1.4×10^{12} cm^{-2} gives $dN_0/dN_s = 0.73$ and $dN_1/dN_s = 0.27$ in the InAs inversion layers. This figure also indicates that the three-subband conduction state is realized above an N_s of about $(7-8)\times10^{12}$ cm^{-2} in InAs.

Figure 5(b) plots the result (solid circles) for InP samples. Here, the open circles represent the results obtained from the magnetoconductance data ($d\sigma/dB$ versus B) under the fixed-gate voltage condition, using the relation

$$N_\nu = n_\nu e/\pi\hbar\Delta(1/B)_\nu \,.$$

It can be seen here that the two-subband conduction state

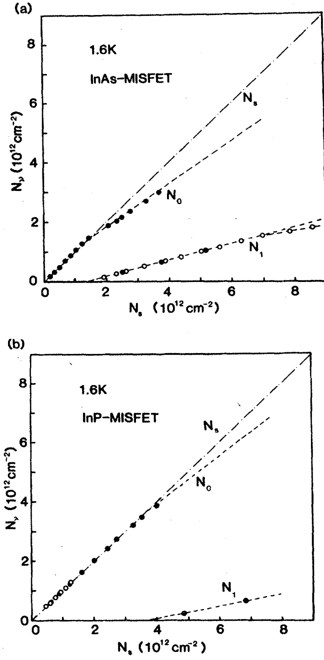

FIG. 5. Conduction-electron concentration in each subband, N_ν, as a function of induced electron concentration N_s at 1.6 K for (a) InAs and (b) InP.

above an N_s of 3.8×10^{12} cm^{-2} gives $dN_0/dN_s=0.79$ and $dN_1/dN_s=0.21$ in the InP inversion layers.

Chen and Koch reported that the two-subband conduction state is realized above an N_s of about 1×10^{12} cm^{-2} both in accumulation and inversion layers on InP MIS diodes.[28] This disagreement may be due to the fact that they used the light-emitted-diode (LED) illumination.

B. Mobility

Conductivity σ as a function of N_s provides the effective mobility μ_{eff} and the field-effect mobility μ_{FE}, using the definition

$$\mu_{\text{eff}}=\sigma/eN_s=\sigma/C_i(V_g-V_{\text{th}}) \tag{7}$$

and

$$\mu_{\text{FE}}=\partial\sigma/C_i\partial V_g \ . \tag{8}$$

As can readily be seen from Eq. (7), when $N_s=N_{\text{inv}}$, μ_{eff} is exactly equal to the drift mobility μ given by σ/eN_{inv}. Incidentally, when quantum effects involving the weak localization effect can be neglected, conductivity σ, as a function of B, for the samples with Corbino-disk structures yields the magnetoresistance mobility $\tilde{\mu}_H$ with the Corbino magnetoresistance effect

$$\Delta\rho(B)/\rho(0)=\tilde{\mu}_H^2B^2 \ , \tag{9}$$

where $\rho(B)=1/\sigma(B)$ and $\Delta\rho(B)=\rho(B)-\rho(0)$. At low temperatures, drift mobility μ, Hall mobility μ_H, and magnetoresistance mobility $\tilde{\mu}_H$, are given by

$$\mu=\sum_\nu N_\nu\mu_\nu/N_{\text{inv}} \ , \tag{10a}$$

$$\mu_H=\sum_\nu N_\nu\mu_\nu^2\Big/\sum_\nu N_\nu\mu_\nu \ , \tag{10b}$$

and

$$\tilde{\mu}_H=\left[\sum_\nu N_\nu\mu_\nu^3\Big/\sum_\nu N_\nu\mu_\nu\right]^{1/2} \tag{10c}$$

with the νth subband electron mobility μ_ν. Therefore, the following relationships can be obtained:

$$\tilde{\mu}_H-\mu=\begin{cases}0 \ \text{(one-subband)}, & \text{(11a)}\\ C(\mu_0-\mu_1)^2\geq 0 \ \text{(two-subband)}, & \text{(11b)}\end{cases}$$

where

$$C=N_0N_1(\mu\tilde{\mu}_H+\mu\mu_H+\mu_0\mu_1)/N_{\text{inv}}^2\mu^2(\tilde{\mu}_H+\mu_H) \ . \tag{12}$$

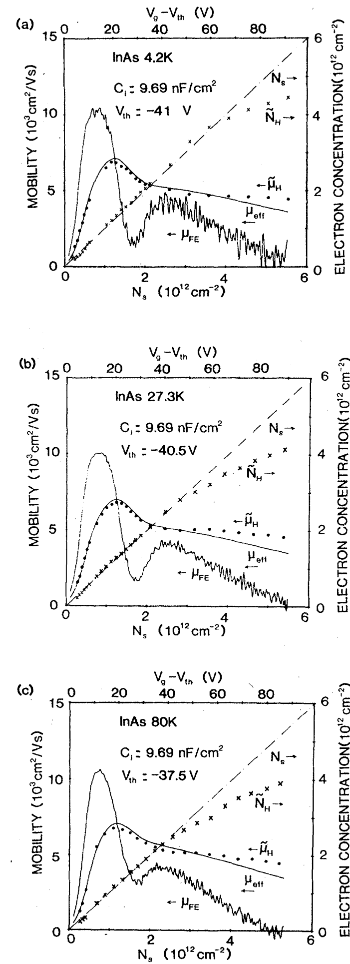

FIG. 6. Mobilities μ_{eff}, μ_{FE}, and $\tilde{\mu}_H$, and magnetoresistance concentration $\tilde{N}_H$, as a function of induced electron concentration N_s in an InAs MISFET (A-2) at (a) 4.2 K, (b) 27.3 K, and (c) 80 K.

Figures 6 and 7 show the experimental results of mobilities $\mu_{\rm eff}$, $\mu_{\rm FE}$, and $\tilde{\mu}_H$ (Ref. 30) as a function of N_s for various temperatures T in the InAs and InP MISFET's, respectively, where magnetoresistance electron concentrations $\tilde{N}_H$, defined by $\sigma/e\tilde{\mu}_H$, are also plotted.

The following results can be obtained from these figures.

(a) Field-effect mobility $\mu_{\rm FE}$ abruptly decreases at the onset of the two-subband conduction equal to an N_s of 1.4×10^{12} cm^{-2} for InAs and 3.8×10^{12} cm^{-2} for InP at low temperatures. This remarkable effect is due to intersubband scattering.[31]

(b) Effective-mobility $\mu_{\rm eff}$ is equal to magnetoresistance mobility $\tilde{\mu}_H$ in the one-subband conduction region below about 80 K. This result again proves the relationship $N_s=N_{\rm inv}$. On the other hand, $\mu_{\rm eff}$ is always smaller than $\tilde{\mu}_H$ in the two-subband conduction region, which leads to the fact $\mu_0\neq\mu_1$, as shown in Eq. (11b).

(c) Mobilities in the intermediate-to-high N_s region ($N_s\gtrsim10^{12}$ cm^{-2}) are almost completely independent of temperatures below 80 K. It can therefore be considered that scatterers have short-range potentials which provide Born amplitudes almost independent of the 2D wave vector **k** in this region.

Figures 8(a) and 8(b) demonstrate the N_s dependence of effective mobility $\mu_{\rm eff}$ for various InAs samples at 77 K and an InP sample at several T's, respectively (solid lines). Here, note that $\mu_{\rm eff}$ has been found to be equal to drift mobility μ, because of the relation $N_s=N_{\rm inv}$, as shown in Sec. III A. These figures also show the calculated results of mobility, where $\mu_{\rm sc}$, $\mu_{\rm def}$, and μ_{SR} represent the calculated mobility limited by Coulomb scattering with charged interface states,[32] defect scattering due to out-diffusion of group-V atoms,[33] and surface-roughness scattering,[34] respectively. Table II summarizes the parameter values used in these calculations, where

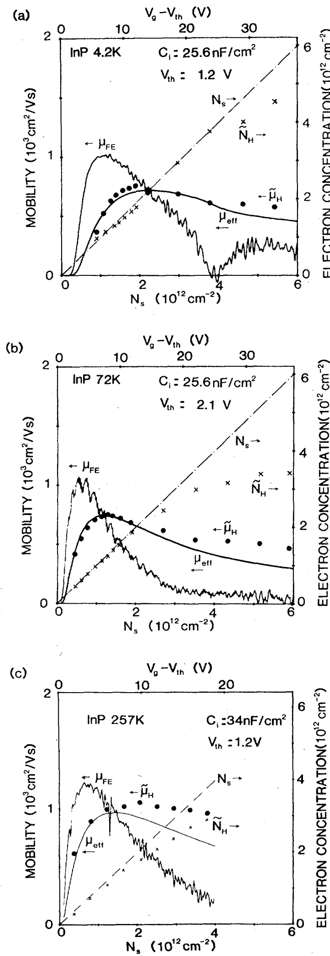

FIG. 7. Mobilities, $\mu_{\rm eff}$, $\mu_{\rm FE}$, and $\tilde{\mu}_H$, and magnetoresistance electron concentration $\tilde{N}_H$, as a function of induced electron concentration N_s in an InP MISFET (P-1) at (a) 4.2 K, (b) 72 K, and (c) 257 K.

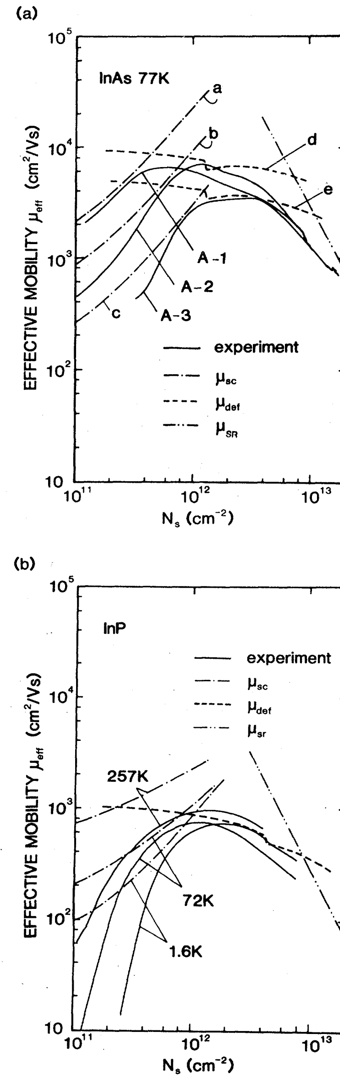

FIG. 8. Effective mobility $\mu_{\rm eff}$ as a function of N_s (a) for various InAs samples at 77 K and (b) for an InP sample at several temperatures. Here, $\mu_{\rm sc}$, $\mu_{\rm def}$, and $\mu_{\rm SR}$ denote the calculated results of mobilities limited by screened Coulomb scattering, defect scattering, and surface-roughness scattering, respectively.

TABLE II. Parameters used in the calculations shown in Fig. 8.

Sample	μ_{sc} N_{int} (cm^{-2})		N_{sc} (cm^{-3})
InAs a	3.5×10^{12}		1×10^{17}
b	9×10^{12}		1×10^{17}
c	3×10^{13}		1×10^{17}
InP	9×10^{12}		1.7×10^{16}
Sample	μ_{def} $N_0U_0^2$ (e^2V^2 cm^3)	a_0 (Å)	δ^{-1} (Å)
InAs d	5.6×10^{-22}	15	100
e	1.0×10^{-21}	15	100
InP	2.7×10^{-22}	15	100
Sample	μ_{SR} L (Å)		Δ (Å)
InAs	30		13
InP	30		13

N_{int} and N_{sc} are concentrations of the charge interface states and acceptor states, respectively, N_0 and U_0 are, respectively, the defect concentration at the semiconductor surface and defect potential, a_0 is the defect potential range, δ^{-1} is the out-diffusion length, and L and Δ are, respectively, the correlation length and average amplitude of surface roughness. As shown in these figures, in the low-N_s region ($N_s < 10^{12}$ cm^{-2}), μ_{eff} strongly increases with an increase in N_s. The good agreement between the experiment and the theory indicates that, in this region, μ_{eff} is mainly limited by the Coulomb scattering due to the charged interface states, which becomes screened with an increase in N_{inv}. On the other hand, in the high-N_s region ($N_s \gtrsim 6\times10^{12}$ cm^{-2}), μ_{eff} strongly decreases in proportion to $N_s^{-(1.3-1.5)}$, which signifies the existence of the surface-roughness-scattering effect at higher N_s values. In the intermediate-N_s region ($10^{12} \lesssim N_s < 6\times10^{12}$ cm^{-2}), μ_{eff} can be considered to be mainly limited by the scattering with defects induced by the out-diffusion of group-V atoms. It has further been found in Fig. 8(a) that μ_{eff} strongly depends on the deposition temperatures in the low and intermediate regions, while the mobility is almost completely independent of sample-preparation conditions in the high-N_s region. Therefore, it is considered that the defect at semiconductor interface which may bring the charged interface states is produced through the pyrolytic growth of gate insulators.

C. Magnetoconductivity

As is well known in disordered 2DEG systems, a long inelastic scattering time τ_ϵ yields quantum interference in extended states, which gives a logarithmic increase of resistivity with a decrease in temperature.[35,36] Hikami, Larkin, and Nagaoka found that this weak localization effect also causes a negative magnetoresistance at low temperatures, because the time-reversal symmetry for the quantum interference is destroyed by applying the magnetic field.[37]

They further found that spin-orbit scattering gives rise to a remarkable effect on the weak localization, that is, a logarithmic increase of 2DEG conductivity with a decrease in temperature as well as a positive magnetoresistance at low temperatures. They therefore introduced the following formula:

$$\Delta\sigma(B) = -\frac{n_v e^2}{2\pi^2\hbar}\{\Psi(\tfrac{1}{2}+B_0/B) - \Psi(\tfrac{1}{2}+B_1/B) + \Psi(\tfrac{1}{2}+B_2/B)/2 - \Psi(\tfrac{1}{2}+B_3/B)/2 - \ln[B_0(B_2)^{1/2}/B_1(B_3)^{1/2}]\} \quad (B < B_0), \tag{13}$$

where

$$B_0 = \hbar/4eD\tau, \tag{14a}$$

$$B_1 = B_0\tau(1/\tau_\epsilon + 2/\tau_{SO}^z + 2/\tau_{SO}^x), \tag{14b}$$

$$B_2 = B_0\tau/\tau_\epsilon, \tag{14c}$$

and

$$B_3 = B_0\tau(1/\tau_\epsilon + 4/\tau_{SO}^x), \tag{14d}$$

when magnetic impurities are absent. Here, Ψ is the digamma function, D is the diffusion constant, τ is the elastic scattering time, and τ_{SO}^i ($i = x,z$) the i component of the spin-orbit scattering time. It can readily be seen from this formula that the existence of spin-orbit scattering yields a positive magnetoresistance at low magnetic fields ($B < B_3$).

Corbino magnetoconductivity of InAs and InP MISFET's is plotted in Figs. 9(a) and 9(b) as a function of B, at 1.6 K. These figures also show the calculated results of Eq. (13) and Eq. (14) as solid lines, where fitting parameters τ_ϵ and τ_{SO}^i are summarized in the figures and the distinction between the x and z components of the latter are neglected for simplicity. The dotted lines correspond to $\Delta\sigma(B)$ calculated in the region $B \geq B_0$, where Eq. (13) cannot hold. Here, note that $\Delta\sigma(B)$ in Eq. (13), which corresponds to $\Delta(1/\rho_{xx})$, is equal to the Corbino magnetoconductivity only when $B \to 0$. Therefore, τ_ϵ and τ_{SO}^i were determined using the data at $B \simeq 0$ in this work.

It can be seen from these figures that positive magnetoresistance clearly appears at very low B values in the InAs inversion layers, while on the other hand, only negative magnetoresistance is observed in those of InP. In general, magnitudes of spin-orbit interactions are propor-

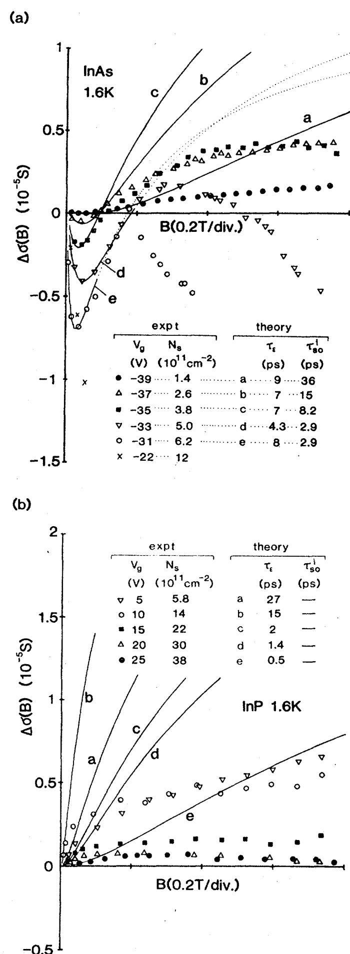

FIG. 9. Magnetoconductivity $\Delta\sigma(B)$ versus magnetic field B at 1.6 K for (a) InAs and (b) InP.

tional to $(g-2)^2$ with effective g factor g,[38] where g values are estimated at -23 and 1.6 for InAs and InP, respectively. It can therefore be considered that this positive magnetoresistance is due to sufficiently large shift of the g factor from 2 in InAs. However, Poole, Pepper, and Hughes recently reported that positive magnetoresistance was observed in InP inversion layers with very low mobility (100—300 $cm^2/V\,s$).[39] They discussed the possibility that the spin-orbit scattering originates from Zn ions or the host lattice. This problem must remain for future investigation.

As shown in Figs. 9(a) and 9(b), precise agreement could not be obtained in high-B regions especially in InP. Therefore, Eq. (13) with fitting parameters τ_ϵ and τ_{SO}^i was fitted to the experimental results at very-low-B regions. Figure 10 shows the obtained results of τ_ϵ and τ_{SO}^i as a function of N_s for various T values. Here it should be noted that the results at 4.2 K, which are not plotted in this figure, are almost equal to the results at 1.6 K. This may be because at 1.6 K the electron temperature is a little larger than T due to the high source-drain field (3 V/cm).

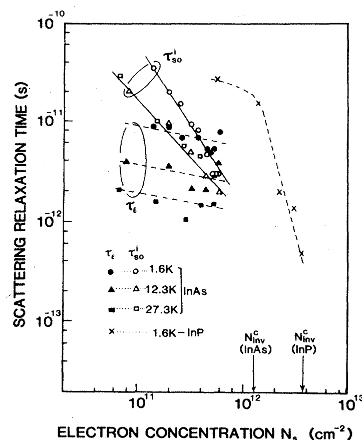

FIG. 10. Inelastic scattering time τ_ϵ and spin-orbit scattering time τ_{SO}^i as a function of induced electron concentration N_s at several T values.

It is concluded that τ_ϵ is roughly proportional to $N_s^{-(0-0.2)}T^{-1}$ for $N_s < 10^{12}$ cm^{-2} and $T \geq 4.2$ K. On the other hand, τ_{SO}^i is found to strongly depend on N_s, roughly proportional to $N_s^{-(0.8-1.6)}T^{-(0-0.4)}$ for $N_s < 10^{12}$ cm^{-2}. Furthermore, this figure clearly shows that τ_ϵ abruptly decreases as N_s approaches N_{inv}^c (the onset concentration of the two-subband conduction state). It can thus be considered that intersubband scattering also gives rise to a remarkable effect on the inelastic scattering time, i.e., weak localization.[33]

IV. CONCLUSION

This final section provides a summary of the conclusions on the electron subbands and transport properties in inversion layers on III-V compound semiconductors InAs and InP. Apparent SdH oscillations have been observed on both the InAs and InP inversion layers (Fig. 2). Fan diagrams shown in Fig. 3 prove not only good two dimensionality, but also the absence of the band-tailing effect on the surfaces of these III-V compounds.

Analysis for the SdH effect have given the following results on the subband structures. Conduction-electron concentration N_{inv} is exactly equal to induced electron concentration N_s in any sample. The first excited subband becomes occupied above an N_s of 1.4×10^{12} and 3.8×10^{12} cm^{-2} for InAs and InP, respectively. The second excited subband becomes occupied above an N_s of $(7-8)\times10^{12}$ cm^{-2} for InAs. The occupancy of each subband has been determined, as shown in Fig. 5.

It has been found that field-effect mobility μ_{FE} abruptly decreases just at the onset of the two-subband conduction state, equal to an N_s of 1.4×10^{12} and 3.8×10^{12} cm^{-2} for InAs and InP, respectively, as shown in Figs. 6 and 7. This remarkable effect has been found to be due to intersubband scattering.

The systematic studies on mobilities yield the following

results. In the one-subband conduction regions, the effective mobility μ_{eff} is exactly equal to magnetoresistance mobility, $\tilde{\mu}_H$. This again proves the relation $N_{\text{inv}}=N_s$. On the other hand, in the two-subband conduction regions, μ_{eff} becomes smaller than $\tilde{\mu}_H$ as N_s increases. This result reveals that electron mobility of the excited subband, μ_1, is different from that of the ground subband, μ_0.

Mobilities at low-N_s regions ($<10^{12}$ cm^{-2}) strongly depend on sample-preparation conditions. Theoretical studies have indicated that the mobilities in these regions are limited by screened Coulomb scattering due to charged interface states. Mobilities at high-N_s regions ($\geq 6\times 10^{12}$ cm^{-2}) are almost proportional to $N_s^{-(1.3-1.5)}$, and independent of temperatures and sample-preparation conditions. This suggests the existence of a surface-roughness-scattering effect at higher N_s values. On the other hand, mobilities at intermediate-N_s regions ($10^{12} \leq N_s < 6\times 10^{12}$ cm^{-2}), which are also independent of temperatures, strongly depend on sample-preparation conditions, especially on insulator deposition temperatures. A simple model concerning the defect scattering due to the outdiffusion of group-V atoms can phenomenologically explain these behaviors for mobilities at these intermediate-N_s regions (Fig. 8).

Furthermore, negative magnetoresistance due to weak localization has been observed in the 2D inversion layers for both InAs and InP. Positive magnetoresistance has also been observed, due to spin-orbit interactions, in the InAs inversion layers (Fig. 9). Values for the characteristic relaxation times, τ_ϵ and τ^i_{SO}, have been obtained as functions of N_s and T, although the theory appears inadequate (Fig. 10). It has been found that intersubband scattering gives rise to a remarkable effect on the weak localization.

ACKNOWLEDGMENTS

I would like to thank Professor Tsuneya Ando for his many valuable discussions and comments. I am indepted to Professor Shinji Kawaji, Professor Hiroyuki Sakaki, and Dr. Hideo Aoki for their helpful advice. My appreciation also goes not only to Dr. Yoshitaka Furukawa, Dr. Osamu Mikami, Dr. Yukinobu Shinoda, and Mr. Masamichi Okamura for their stimulating discussions and technical advice, but also to Ms. Tomoko Hisaki for her photolithography assistance.

*Permanent address.

[1]D. L. Lile, D. A. Collins, L. G. Meiners, and L. Messick, Electron. Lett. **14**, 657 (1978).

[2]T. Kawakami and M. Okamura, Electron. Lett. **15**, 502 (1979).

[3]D. Fritzsche, in *Proceedings of the Symposium on Insulating Films on Semiconductors, Durham, 1979,* edited by G. G. Roberts and M. J. Morant (IOP, Bristol, 1980) [Inst. Phys. Conf. Ser. **50**, 258 (1980)].

[4]T. Sawada, K. Ishii, and H. Hasegewa, Jpn. J. Appl. Phys. **21**, Suppl. 21-1, 397 (1981).

[5]K. Ohata, T. Itoh, H. Watanabe, T. Mizutani, and Y. Takayama, in *Proceedings of Symposium on GaAs and Related Compounds,* Oiso, 1981 edited by T. Sugano (IOP Bristol, 1981) [Inst. Phys. Conf. Ser. **63**, 353 (1982)].

[6]A. Yamamoto and C. Uemura, Electron. Lett. **18**, 63 (1982).

[7]T. Kobayashi and Y. Hirota, Electron. Lett. **18**, 180 (1982).

[8]Y. Hirayama, H. M. Park, F. Koshiga, and T. Sugano, Appl. Phys. Lett. **40**, 712 (1982).

[9]E. Yamaguchi, Y. Hirota, and M. Minakata, Thin Solid Films **103**, 201 (1983).

[10]E. Yamaguchi, M. Minakata, and Y. Furukawa, Jpn. J. Appl. Phys. **19**, 2301 (1980).

[11]H. H. Wieder, in *Proceedings of the Symposium on Insulating Films on Semiconductors, Durham, 1979,* edited by G. G. Roberts and M. J. Morant (IOP, Bristol, 1980) [Inst. Phys. Conf. Ser. **50**, 2349 (1980)].

[12]Y. Shinoda, M. Okamura, E. Yamaguchi, and T. Kobayashi, Jpn. J. Appl. Phys. **19**, 2301 (1980).

[13]A. S. H. Liao, B. Tell, R. F. Lehny, and T. Y. Chang, Appl. Phys. Lett. **41**, 280 (1982).

[14]H. Terao, T. Ito, and Y. Sakai, J. Electr. Eng. Jpn. **94**, 127 (1974).

[15]D. A. Baglee, D. K. Ferry, C. W. Wilmsen, and H. H. Wieder, J. Vac. Sci. Technol. **17**, 1032 (1980).

[16]E. Yamaguchi and M. Minakata, Appl. Phys. Lett. **43**, 965 (1983).

[17]D. C. Tsui, Solid State Commun. **8**, 113 (1970).

[18]D. C. Tsui, Phys. Rev. Lett. **24**, 303 (1970).

[19]D. C. Tsui, Phys. Rev. B **4**, 4438 (1971).

[20]D. C. Tsui, Phys. Rev. B **8**, 2657 (1973).

[21]D. C. Tsui, Phys. Rev. B **12**, 5739 (1975).

[22]H. Sakai, L. L. Chang, G. A. Sai-Halasz, C. A. Chang, and L. Esaki, Solid State Commun. **26**, 589 (1978).

[23]H. A. Washburn and J. R. Sites, Surf. Sci. **73**, 537 (1978).

[24]H. A. Washburn, J. R. Sites, and H. H. Wieder, J. Appl. Phys. **50**, 4872 (1979).

[25]S. Kawaji and Y. Kawaguchi, in *Proceedings of the International Conference on the Physics of Semiconductors, Kyoto, 1966* [J. Phys. Soc. Jpn. **21**, 336 (1966)].

[26]S. Kawaji and H. C. Gatos, Surf. Sci. **7**, 215 (1967).

[27]K. v. Klitzing, T. Englert, and D. Fritzsche, J. Appl. Phys. **51**, 5893 (1980); K. v. Klitzing, T. Englert, E. Bangert, and D. Fritzsche, in *Proceedings of the International Conference on the Physics of Semiconductors, Kyoto, 1980* [J. Phys. Soc. Jpn. **49**, Suppl. A, 979 (1980)].

[28]H. C. Cheng and F. Koch, Solid State Commun. **37**, 911 (1981); Phys. Rev. B **26**, 1989 (1982).

[29]E. Yamaguchi, in *Extended Abstract of the International Conference on Solid State Devices and Materials, Kobe, 1984* (Japan Society of Applied Physics, Tokyo, 1984), p. 371.

[30]As reported in Sec. III C, the weak localization effect has been found to give the conductivity correction $\Delta\sigma(B)$ at low temperatures in both InAs and InP. The correction term $\Delta\sigma(B)$ is such a slowly varying function of B at large B that $\tilde{\mu}_H$ has roughly been estimated by taking the almost constant correction term from the observed conductivity in sufficiently large B regions.

[31]S. Mori and T. Ando, Phys. Rev. B **19**, 6433 (1979).

[32]F. Stern and W. E. Howard, Phys. Rev. **163**, 816 (1967).

[33]E. Yamaguchi, J. Appl. Phys. **56**, 1722 (1984).

[34]Y. Matsumoto and Y. Uemura, in *Proceedings of the International Conference on Solid Surfaces,* Kyoto, 1974 [Jpn. J. Appl. Phys. Suppl. 2, Part 2, 367 (1974)].

[35]E. Abrahams, P. W. Anderson, D. C. Liciardelo, and T. V.

Ramarkrishnan, Phys. Rev. Lett. **42**, 673 (1979).
[36]L. P. Gor'kov, A. I. Larkin, and Khmel'nitskii, Pis'ma Zh. Eksp. Teor. Fiz. **30**, 248 (1979) [JETP Lett. **30**, 228 (1979)].
[37]S. Hikami, A. I. Larkin, and Y. Nagaoka, Prog. Theor. Phys. **63**, 707 (1980).
[38]R. J. Elliott, Phys. Rev. **96**, 266 (1954).
[39]D. A. Poole, M. Pepper, and A. Hughes, J. Phys. C **15**, L1137 (1982).